European Radiology
https://doi.org/10.1007/s00330-017-5213-1

ONCOLOGY

^{18}F-Fluciclovine PET/MRI for preoperative lymph node staging in high-risk prostate cancer patients

Kirsten M. Selnæs[1,2] · Brage Krüger-Stokke[1,2] · Mattijs Elschot[1] · Frode Willoch[3] · Øystein Størkersen[4] · Elise Sandsmark[1] · Siver A. Moestue[1] · May-Britt Tessem[1] · Dag Halvorsen[5] · Eirik Kjøbli[5] · Anders Angelsen[6] · Sverre Langørgen[2] · Helena Bertilsson[5,7] · Tone F. Bathen[1]

Received: 13 July 2017 / Revised: 17 November 2017 / Accepted: 24 November 2017

Abstract

Objective To investigate the diagnostic potential of simultaneous ^{18}F-fluciclovine PET/MRI for pelvic lymph node (LN) staging in patients with high-risk prostate cancer.

Methods High-risk prostate cancer patients (n=28) underwent simultaneous ^{18}F-fluciclovine PET/MRI prior to surgery. LNs were removed according to a predefined template of eight regions. PET and MR images were evaluated for presence of LN metastases according to these regions. Sensitivity/specificity for detection of LN metastases were calculated on patient and region basis. Sizes of LN metastases in regions with positive and negative imaging findings were compared with linear mixed models. Clinical parameters of PET-positive and -negative stage N1 patients were compared with the Mann-Whitney U test.

Results Patient- and region-based sensitivity/specificity for detection of pelvic LN metastases was 40 %/87.5 % and 35 %/95.7 %, respectively, for MRI and 40 %/100 % and 30 %/100 %, respectively, for PET. LN metastases in true-positive regions were significantly larger than metastases in false-negative regions. PET-positive stage N1 patients had higher metastatic burden than PET-negative N1 patients.

Conclusion Simultaneous ^{18}F-fluciclovine PET/MRI provides high specificity but low sensitivity for detection of LN metastases in high-risk prostate cancer patients. ^{18}F-Fluciclovine PET/MRI scan positive for LN metastases indicates higher metastatic burden than negative scan.

Key Points

- *^{18}F-Fluciclovine PET/MRI has high specificity for detection of lymph node metastasis.*
- *^{18}F-Fluciclovine PET/MRI lacks sensitivity to replace ePLND.*
- *^{18}F-Fluciclovine PET/MRI may be used to aid surgery and select adjuvant therapy.*
- *^{18}F-Fluciclovine PET-positive patients have more extensive disease than PET-negative patients.*
- *Size of metastatic lymph nodes is an important factor for detection.*

Kirsten M. Selnæs and Brage Krüger-Stokke contributed equally to this work.

Electronic supplementary material The online version of this article (https://doi.org/10.1007/s00330-017-5213-1) contains supplementary material, which is available to authorized users.

✉ Kirsten M. Selnæs
kirsten.m.selnas@ntnu.no

[1] Department of Circulation and Medical Imaging, Faculty of Medicine and Health Sciences, NTNU – Norwegian University of Science and Technology, Post box 8905, MTFS, 7491 Trondheim, Norway

[2] Department of Radiology, St. Olavs Hospital, Trondheim University Hospital, Trondheim, Norway

[3] Institute of Basic Medical Sciences, Faculty of Medicine, University of Oslo, Oslo, Norway

[4] Department of Pathology and Medical Genetics, St. Olavs Hospital, Trondheim University Hospital, Trondheim, Norway

[5] Department of Urology, St. Olavs Hospital, Trondheim University Hospital, Trondheim, Norway

[6] Urologiklinikken AS, Nøtterøy, Norway

[7] Department of Cancer Research and Molecular Medicine, Faculty of Medicine and Health Sciences, NTNU – Norwegian University of Science and Technology, Trondheim, Norway

Published online: 02 January 2018

Keywords Positron-emission tomography · Magnetic resonance imaging · FACBC · Adenocarcinoma · N-staging

Abbreviations

AC	Attenuation correction
BP1	Bed position 1
BP2	Bed position 2
CT	Computed tomography
DCE	Dynamic contrast-enhanced
DWI	Diffusion-weighted imaging
ePLND	Extended pelvic LN dissection
FN	False negative
FP	False positive
GS	Gleason score
ITD	Index tumour diameter
LN	Lymph node
MRI	Magnetic resonance imaging
MRSI	Magnetic resonance spectroscopic imaging
NPV	Negative predictive value
PET	Positron emission tomography
PPV	Positive-predictive value
PRESS	Point RESolved Spectroscopy
RARP	Robot-assisted radical prostatectomy
SPACE	Sampling perfection with application-optimized contrasts using different flip angle evolution
SS-EPI	Single-shot echo planar imaging
T1W	T1-weighted
T2W	T2-weighted
TE	Echo time
TN	True negative
TP	True positive
TR	Repetition time
TSE	Turbo spin cho
VIBE	Volume interpolated gradient echo

Introduction

Accurate diagnosis of lymph node (LN) metastases remains a challenge in prostate cancer. The sensitivity of conventional imaging with computed tomography (CT) and magnetic resonance imaging (MRI) is unsatisfactory [1], leaving extended pelvic LN dissection (ePLND) the most accurate method for staging [2]. However, ePLND can be associated with longer hospital stays, operative time and an overall higher rate of complications compared to limited pelvic LN dissection [3]. A patient-tailored approach with accurate preoperative detection of LN metastases could potentially reduce the extent of LN dissection or guide the surgeon to potential metastases outside the standard surgical template.

Several studies have indicated that positron emission tomography (PET) may play a role in both staging of primary prostate cancer and detection of disease after biochemical relapse [4–6]. Although promising, currently available radiotracers have yet to show acceptable sensitivities for staging in routine clinical use. PET/CT with choline-based radiotracers have shown sensitivities in the range of 45–73 % for preoperative staging of LN metastases [7, 8], while ^{68}Gallium-labeled PSMA PET/CT yielded a sensitivity of 65.9 % for detection of LN metastases [9]. Another radiotracer that has shown promise in primary and recurrent prostate cancer imaging is the leucine amino acid analogue anti-1-amino-3-^{18}F-fluorocyclobutane-1-carboxylic acid (^{18}F-fluciclovine, also known as ^{18}F-FACBC), with subject level scan positivity rates in the range of 37–83 % for recurrent disease [5, 10, 11]. ^{18}F-Fluciclovine uptake is mediated by sodium-dependent and -independent pathways associated with cancer signaling pathways [12, 13]. It has the advantage of minimal urinary excretion at early timepoint imaging, and a favourable tumour-to-background ratio [14, 15]. ^{18}F-Fluciclovine was recently approved by the US Food and Drug Administration (FDA) for use in detection of recurrent prostate cancer [16]. The clinical evidence for ^{18}F-fluciclovine in LN staging of primary prostate cancer patients has, however, been less explored, and with study limitations such as small cohorts and lack of histopathology as gold standard [6, 17–19].

Current guidelines for high-risk prostate cancer warrant multiparametric MRI for local T-staging and cross-sectional imaging and bone scans for N- and M-staging [2]. Cross-sectional imaging obtained from CT is of limited diagnostic value in prostate cancer, ultimately leading to additional confirmatory imaging with MRI and biopsies. With the advent of integrated PET/MRI scanners, we are able to acquire MR images of diagnostic quality and metabolic PET data in one examination, saving the patient from enduring several separate examinations. The purpose of this study was to investigate the diagnostic potential of simultaneous ^{18}F-fluciclovine PET/MRI for LN staging in patients with high-risk prostate cancer using an all-in-one imaging protocol.

Materials and methods

Patients

The Regional Committee of Medical and Health Research Ethics, Central Norway (identifier 2013/1513), approved this prospective study (ClinicalTrials.gov; identifier NCT02076503). Written and oral informed consent was collected from all patients included in the study.

Patients (n=28) scheduled for robot-assisted radical prostatectomy (RARP) with ePLND underwent simultaneous ^{18}F-fluciclovine PET/MRI at St. Olavs Hospital, Trondheim University Hospital, between May 2014 and September

2015. At the time of inclusion all patients were classified as high-risk according to modified D'Amico criteria (PSA > 20 ng/ml and/or clinical stage ≥ cT3 and/or Gleason score ≥ 8) [20]. Exclusion criteria were general contraindications to MRI, previous or ongoing androgen deprivation therapy and previous prostatic surgery. Two patients did not undergo ePLND due to down-staging by MRI, leaving a total of 26 patients for analysis (Fig. 1).

PET/MRI protocol

Patients were imaged with a 3.0T PET/MRI scanner (Magnetom Biograph mMR, Siemens Medical Systems, Erlangen, Germany) as previously described [15]. In short, the imaging protocol was designed to yield diagnostic MR images of the prostate and pelvis from the ureteral crossing of the common iliac vessels to the pelvic floor in two bed positions. T2-weighted images, diffusion-weighted images, magnetic resonance spectroscopic imaging and dynamic contrast-enhanced images were acquired for evaluation of the prostate gland. Coronal T1-weighted images were acquired for detection of skeletal metastases while coronal diffusion-weighted images and a 3D T2-weighted sequence were acquired for detection and characterization of LNs. A total of 45 min of sequential list-mode PET data were acquired over the pelvic region, from which PET images binned over 5–10 min post-injection were reconstructed for interpretation using a manufacturer-provided algorithm (OSEM, 4 iterations, 21 subsets, 6-mm Gaussian post-reconstruction filter). The acquisition protocol is presented in Table 1.

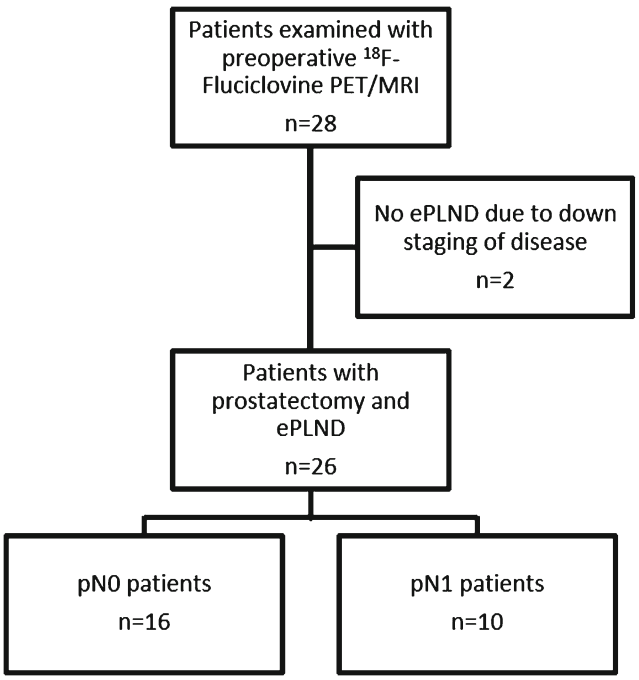

Fig. 1 Flowchart of the study population. *ePLND* extended pelvic lymph node dissection, *pN0* pathological stage N0, *pN1* pathological stage N1

Surgery and histopathology

RARP with ePLND was performed by three board-certified urological surgeons according to EAU guidelines [2]. The surgeons had access to the initial MRI reading and clinical data, but were blinded to the PET-results. The prostate gland was removed as a whole and LNs were removed according to a predefined surgical template of eight anatomical regions (four on each side of the pelvis) [21]. The resected tissue was sent for histopathological analysis in separate containers, one for the prostate and one container for each LN region. Resected tissue was fixed in 4 % buffered formaldehyde before further analysis. The prostate was serially sectioned from apex to base in 4-mm thick slices. LNs ≤ 3 mm were evaluated as a whole, otherwise they were cut in 3- to 4-mm slices. All slices were embedded in paraffin before 3.5-μm thick sections were stained with haematoxylin and eosin. Cancer foci in the prostate were outlined and long- and short-axis diameter of the LNs, size and Gleason score of tumour deposit within the LNs were registered by a dedicated pathologist with 10 years of experience in uropathology (Ø.S). If two or more regions were not separated at surgery, we regarded them as one fused region in case of metastases. In cases where a region contained more than one metastatic LN, only the largest was used for comparison with imaging results.

Image interpretation

Absence or presence of LN metastases was evaluated with an anatomical region-based approach (corresponding to the surgical template for ePLND), since comparison of imaging to histopathology on a LN level was deemed impossible.

MR images were interpreted by a board-certified radiologist (S.L.) and a radiology resident (B.K.-S.) with 5 and 1 years of experience, respectively, in reading prostate MRI. Radiologists were blinded to PET images, but had access to relevant clinical information. In case of disagreement, consensus was reached by re-examining the images. Regions corresponding to the surgical template for ePLND were scored as 1 – non-metastatic, 2 – equivocal or 3 – metastatic, at the radiologists' discretion.

Blinded to the initial MRI reading, a board-certified nuclear medicine physician (F.W.) with more than 20 years of PET experience and extensive experience reading ^{18}F-fluciclovine PET/CT, examined the PET images using 3D T2-weighted images for anatomical correlation. Findings were reported as positive or negative per region, using a semi-quantitative criterion of target to blood-pool ratio of ≥ 2.0 in the reconstructed PET image (5–10 min post-injection) for positive findings, based on the reader's experience.

A retrospective evaluation of target-to-blood pool ratio was performed for the most suspicious LN in each of the false

Table 1 Specifications of the PET/MR imaging protocol

Bed position	Time (min)	Sequence	Orientation	TR/TE1/TE2 (ms)	Matrix	No. ofslices	Resolution (mm)	
							In-plane	Slice
BP1	30	*T2W TSE*	*Sagittal*	*5,590/100*	*320 x 320*	*19*	*0.6 x 0.6*	*3.0*
		T2W TSE	*Transverse*	*6,840/104*	*384 x 384*	*23*	*0.5 x 0.5*	*3.0*
		T2W TSE	*Coronal*	*5,470/101*	*320 x 320*	*19*	*0.6 x 0.6*	*3.0*
		DWI (SS-EPI)[a]	*Transverse*	*6,100/67*	*96 x 102*	*23*	*2.5 x 2.5*	*3.0*
Change table position; injection of tracer								
BP2	25	AC (DIXON)	Coronal	3.6/1.2/2.5	192 x 126	128	2.6 x 2.6	3.1
		PET[b]	Transverse	N.A	344 x 344	127	2.1 x 2.1	2.0
		T1W TSE	Coronal	815/10	384 x 384	50	0.9 x 0.9	3.3
		DWI (SS-EPI)[a]	Coronal	10,400/67	98 x 100	40	2.6 x 2.6	4.4
		T2 SPACE	Coronal (3D)	1,500/82	320 x 320	144	1.0 x 1.0	1.1
Change table position								
BP1	20	*DIXON*	*Coronal*	*3.6/1.2/2.5*	*192 x 126*	*128*	*2.6 x 2.6*	*3.1*
		PET[b]	*Transverse*	*N.A*	*344 x 344*	*127*	*2.1 x 2.1*	*2.0*
		MRSI (PRESS)	*Transverse (3D)*	*740/145*	*12 x 12*	*10*	*7.0 x 7.0*	*7.0*
		DCE (T1W VIBE)	*Transverse (3D)*	*4.2/1.0*	*128 x 128*	*26*	*1.8 x 1.8*	*3.0*

Note: Sequences in italic presentation were used for evaluation of the prostate gland

T2W T2-weighted, *TSE* Turbo Spin Echo, *DWI* diffusion-weighted imaging, *SS-EPI* single shot echo planar imaging, *AC* Attenuation correction, *T1W* T1-weighted, *SPACE* Sampling Perfection with Application-optimized Contrasts using different flip angle Evolution, *MRSI* magnetic resonance spectroscopic imaging, *PRESS* Point RESolved Spectroscopy, *DCE* Dynamic contrast enhanced, *VIBE* Volume Interpolated Gradient Echo, *BP1* bed position 1 (prostate in iso-center), *BP2* bed position 2 (cover the prostate and pelvic LNs form pelvic floor to the ureteral crossing of the common iliac vessels), *TR* repetition time, *TE* echo time

[a] b-values 0, 50, 400 and 800 were used

[b] PET data were acquired in list mode

positive MR regions (n=8) and in one LN detected by MRI but missed by PET.

Statistical analysis

Descriptive statistics were calculated on patient and region basis after dichotomization of the 3-point MRI scale. To determine the best cut-off, we applied the Youden index, achieving the best results when categorizing score 1 and 2 as negative, and score 3 as positive (Youden index 0.28 and 0.31 for patient- and region-based analysis, respectively, vs. -0.05 and 0.12 categorizing scores 2 and 3 as positive). Diagnostic accuracies and their confidence intervals were calculated according to *Clinical test performance* [22] in MATLAB (The MathWorks Inc., Natick, MA, USA). For assessment of the difference in LN and metastatic deposit size in true-positive and false-negative regions, linear mixed models with patient as a random effect on the intercept were used to account for several regions per patient. The Mann-Whitney U test was used to compare clinical parameters in PET-negative and PET-positive stage-N1 patients. Unless otherwise stated, all statistical analyses were performed in SPSS (IBM SPSS Statistics 22.0, Armonk, NY, USA).

Results

Patients

Patient characteristics are described in Table 2. Median (range) time from imaging to surgery was 7.5 days (5–21 days).

Lymph node histopathology

A total of 510 LNs were removed from the 26 patients (median = 20, range 8–45 LNs per patient). LN metastases were detected in ten patients in a total of 47 LNs from 20 regions. Out of the ten patients, there were four patients with only one metastasis, three patients with two metastases, one patient with four metastases, one patient with five metastases and one patient with 28 metastases (Fig. 2), adding up to a median (range) of 2 (1–28) LN metastases per patient. The median (range) long axis diameter of metastatic LNs was 11 mm (3–32 mm), while the short-axis diameter was 5 mm (1.6–17 mm). Metastatic deposits within LNs had a median long axis diameter of 8 mm (0.5–31 mm) and short axis diameter of 4 mm (0.2–17 mm). A detailed description of LN sizes is given in Supplementary Table S1.

Table 2 Patient characteristics

N-stage	N0 (n=16)	N1 (n=10)	All patients (n=26)
Age (y)	66.1 (55.0–71.9)	66.5 (63.3–71.3)	66.2 (55.0–71.9)
GS	7 (7–9)	8 (7–9)	8 (7–9)
GS 7 n (%)	10 (62.5)	1 (10)	11 (42.3)
GS 8 n (%)	3 (18.8)	5 (50)	8 (30.8)
GS 9 n (%)	3 (18.8)	4 (40)	7 (26.9)
pT-stage			
pT2c n (%)	7 (43.8)	0 (0)	7 (26.9)
pT3a n (%)	5 (31.3)	2 (20)	7 (26.9)
pT3b n (%)	3 (18.8)	8 (80)	11 (42.3)
pT4 n (%)	1 (6.3)	0 (0)	1 (3.8)
PSA (ng/ml)	16.7 (6.3–56.9)	9.9 (3.7–45.5)	14.6 (3.7–56.9)
ITD (mm)	30.5 (16.0–48.0)	34.0 (22.0–48.0)	31.0 (16.0–48.0)

Values represent median (range) unless otherwise specified

N0 patients without LN metastases, *N1* patients with LN metastases, *ITD* Index tumour diameter in the prostate, *GS* Gleason score after prostatectomy, *pT-stage* pathological T-stage

Imaging results

The radiologists scored 15 regions as metastatic in six patients based on the MR images. Out of these, seven regions in four patients were true positive, yielding a region-based sensitivity of 35 % and specificity of 95.7 %. Patient-based sensitivity and specificity for detection of LN metastases based on MR images were 40 % and 87.5 %, respectively (Table 3).

The nuclear medicine physician identified six regions as metastatic in four patients based on elevated ^{18}F-fluciclovine uptake. All regions were true positive according to histopathology, yielding a region-based sensitivity of 30 % and specificity of 100 % for detection of LN metastases based on PET. Patient-based sensitivity and specificity were 40 % and 100 %, respectively (Table 3).

There was a significant difference in size of LN metastases in true-positive and false-negative regions (Fig. 3). The largest metastatic LN that was not detected by MRI and PET was 9.5 mm in short axis diameter with a metastatic deposit of 12.0 x 7.0 mm. The smallest LNs detected by MRI and PET had metastatic deposits of 13.0 x 8.0 mm and 16.0 x 8.0 mm, respectively (details are given in Supplementary Table S2).

True-positive regions were identical for PET and MRI except for one region true positive on MRI but false negative on PET. The region was missed by PET but found on MRI, and contained a LN that measured 20 x 8 mm (metastatic deposit 13 x 8 mm) on histopathology and had a target to blood-pool ratio of 1.37 in the 5- to 10-min post-injection PET image (Fig. 4). There were no false-positive regions by PET, but eight false-positive regions by MRI. Median target to blood-pool ratio in the most suspicious LN by MRI in each of these regions was 0.95 (range 0.81–1.24).

Clinical characteristics of stage N1-patients (n=10)

The difference in Gleason score, PSA level, T-stage, index tumour diameter in the prostate and metastatic burden (number of LN metastasis and metastatic regions) were compared for PET-negative and -positive stage-N1 patients (Table 4). All PET-positive N1 patients had a pathological T-stage of T3b. A significant difference was found for index tumour diameter in the prostate, with the PET-positive group having larger index lesions (p=0.038). We observed lower PSA levels in the PET-positive group, but the difference was not significant (p=0.171) and there was no difference in Gleason score between the two groups (p=1.0). Patients in the PET-positive group had a higher total number of LN metastases and positive regions, compared to the PET-negative group (p=0.019 and 0.038, respectively). All patients with PET-positive LN metastases had additional LN metastases that were not detected by PET.

Discussion

This prospective study of preoperative pelvic ^{18}F-fluciclovine PET/MRI in high-risk prostate cancer patients demonstrated a

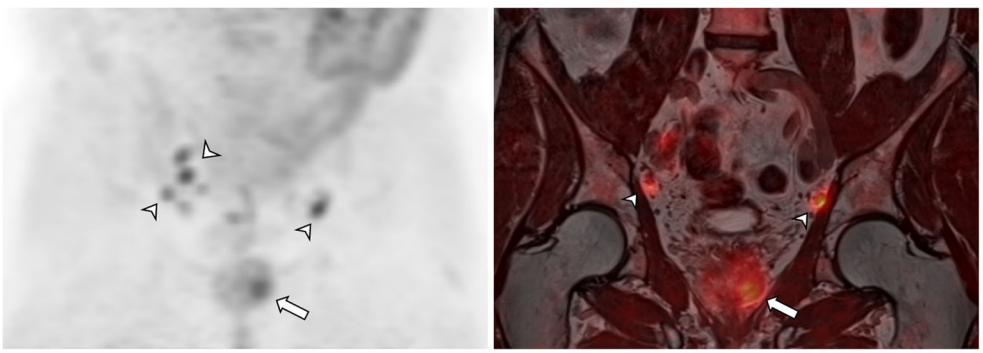

Fig. 2 Preoperative images of a 67-year-old male with prostate cancer (pT3b, Gleason score 4+5, metastatic deposits in 28 of 45 lymph nodes removed by ePLND). Coronal maximum intensity projection from PET (left) and fused PET/MRI (right) shows several of the LN metastases (arrowheads). Note also the activity in the prostate corresponding to the patient's index tumour (arrow)

Table 3 Patient- and region-based diagnostic accuracies

	MRI Patient based	PET	MRI Region based	PET
No. TP	4	4	7	6
No. FP	2	0	8	0
No. FN	6	6	13	14
No. TN	14	16	177	185
Sensitivity	40 % (22.1–60.5)	40.0 % (22.1–60.5)	35 % (28.6–42.0)	30.0 % (23.9–36.8)
Specificity	87.5 % (67.6–97.8)	100 % (84.0–100.0)	95.7 % (91.6–98.0)	100.0 % (97.7–100.0)
PPV	66.7 % (45.6–83.4)	100 % (84.0–100.0)	46. 7 % (39.7–53.7)	100.0 % (97.7–100.0)
NPV	70 % (48.9–86.0)	72.7 % (51.6–88.0)	93.2 % (88.6–96.2)	93.0 % (88.3–96.0)
Accuracy	69.2 % (48.1–85.4)	76.9 % (55.9–91.0)	89.8 % (84.6–93.5)	93.2 % (88.6–96.2)

Numbers in parentheses are 95 % confidence intervals

TP true positive, *FP* false positive, *FN* false negative, *TN* true negative, *PPV* positive predictive value, *NPV* negative predictive value

high specificity but low sensitivity for detection of LN metastases, both on patient level (100 % and 40 %, respectively) and in anatomical regions (100 % and 30 %, respectively). Furthermore, using histopathology as the gold standard, we found that LN metastases below a certain size (8 mm in short axis diameter) were not detected by ^{18}F-fluciclovine PET/MRI at the given SUV threshold, and that the overall burden of LN metastases was higher in patients with positive PET findings.

PET/MRI has the potential to improve initial diagnosis and staging of prostate cancer by combining the excellent soft tissue contrast of MRI with the molecular information from PET in one examination. No previous studies have evaluated the diagnostic accuracy of simultaneous ^{18}F-fluciclovine PET/MRI for preoperative detection of LN metastases in primary prostate cancer patients. It has been demonstrated that LN metastases can be detected by ^{18}F-fluciclovine PET/CT in this patient group, but these studies are limited by a low number of patients and lack of histopathology for evaluation of false-negative findings [14, 17, 19]. In a cohort of radical prostatectomy patients, Suzuki et al. [18] showed that histopathology-proven LN metastases were not detected by preoperative ^{18}F-fluciclovine PET/CT in any of the patients. However, all the LN metastases were 5 mm or smaller, and this is therefore in agreement with our findings.

For PET image interpretation, we applied a rather robust threshold for LN positive findings (target-to-blood pool ratio ≥ 2). With this threshold, there were no false-positive findings in the PET images, resulting in 100 % specificity. With a less conservative threshold, more LN metastases might have been detected. For instance, the one LN metastasis detected by MRI but not by PET had a higher target-to-blood pool ratio (1.37) than LNs in the false-positive MRI regions (median ratio 0.95, range 0.81–1.24). Although based on a limited number of LNs, we could hypothesize that a better threshold for the PET image interpretation could be around 1.3. For small LNs, a size-dependent threshold might be needed in order to identify lesions otherwise impaired by partial volume effect of

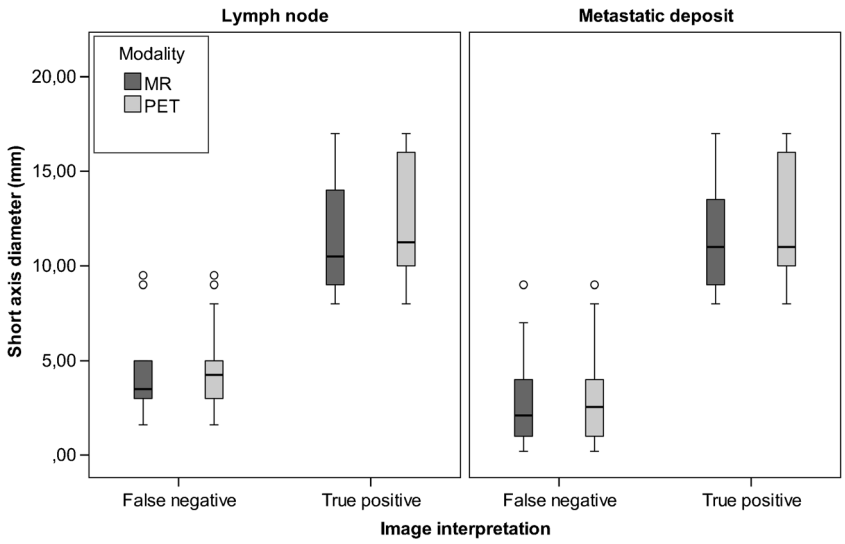

Fig. 3 Short-axis diameter (mm) of lymph nodes and metastatic deposits in true-positive and false-negative regions as evaluated by MRI and PET

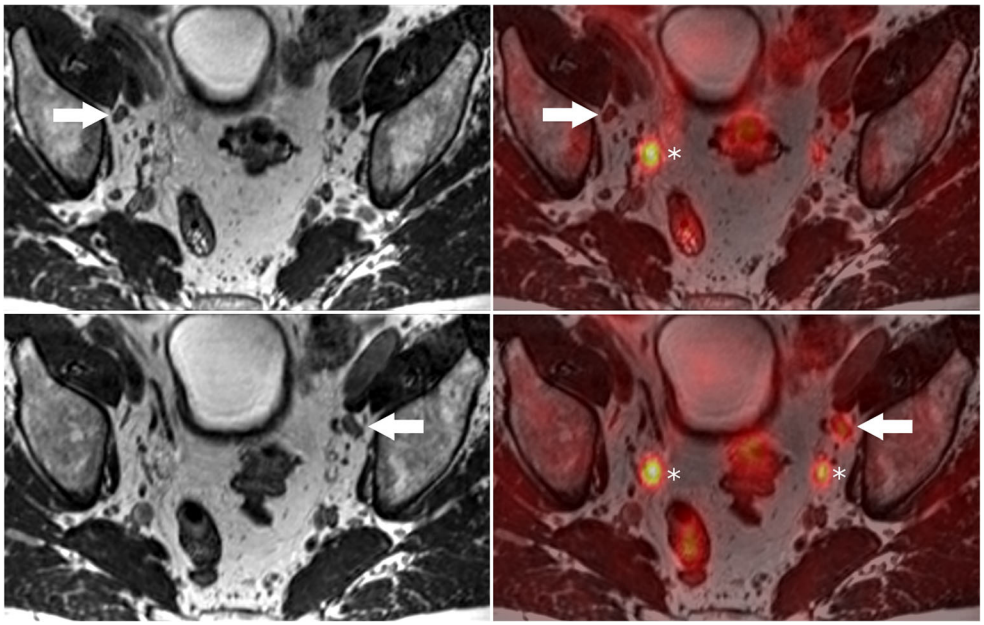

Fig. 4 Preoperative images of a 65-year-old male with prostate cancer (pT3b, Gleason score 4+4, metastatic deposits in four of 21 lymph nodes removed by ePLND). T2W SPACE image (upper left) shows a 10-mm lymph node (LN) (arrow) by the right obturator nerve described as metastasis based on MRI. Fused PET/MR image of the same area (upper right) shows only faint activity in the metastatic LN (target-to-blood pool ratio 1.37). The size of the LN and metastatic deposit measured on histopathology was 20 x 8 mm and 13 x 8 mm, respectively, with Gleason score 4+4. T2W SPACE image (lower left) shows a 10-mm LN (arrow) by the left obturator nerve described as metastasis based on MRI. Fused PET/MR image of the same area (lower right) show tracer uptake in the same LN (target-to-blood pool ratio > 2). The size of the LN and metastatic deposit measured on histopathology was 27 x 12 mm and 18 x 11 mm respectively with Gleason score 4+4. Note the high activity in the ureters (white asterisk) and less intense bowel-uptake

Table 4 Characteristics of PET-positive and -negative pathological stage N1 patients

	PET negative, n=6	PET positive, n=4	*p*-value
GS	8 (7–9)	8.5 (8–9)	1.0
pT-stage (n)			0.476
pT3a	2	0	
pT3b	4	4	
pT4	0	0	
rT-stage (n)			0.114
rT3a	3	0	
rT3b	3	3	
rT4	0	1	
PSA (ng/ml)	10.8 (6.5–45.5)	7.4 (3.7–11.2)	0.171
ITD (mm)	**30 (22–38)**	**46.5 (31–48)**	**0.038**
LNM	**1 (1–2)**	**4.5 (2–28)**	**0.019**
Regions	**1 (1–2)**	**2.5 (2–5)**	**0.038**

Values represent median (range) unless otherwise specified. Bold font indicates a significant difference between PET positive and PET negative patients

GS Gleason score after prostatectomy, *ITD* Index tumour diameter in the prostate, *pT-stage* pathological T-stage, *rT-stage* radiological T-stage, *LNM* number of lymph node metastases, *Regions* number of regions with metastatic lymph nodes

the PET [23]. The vendors of ^{18}F-fluciclovine recommend using uptake equal to or greater than bone marrow as suspicious for large lesions (≥ 1cm), and focal uptake greater than blood pool as suspicious for smaller lesions [24]. These recommendations should, however, be used with caution in PET/MRI since MR-based attenuation correction can lead to underestimation of the SUV value in bone marrow [25]. Finally, other reconstruction methods and time windows might also affect interpretation of the PET images, and further studies are needed in a larger cohort with LN-based analysis to evaluate whether these factors may increase the sensitivity without degrading the specificity.

Our study is in line with previous studies showing high specificity and poor sensitivity for LN detection with PET in high-risk prostate cancer patients [26, 27]. Although other tracers, such as ^{68}Ga-PSMA and ^{18}F-choline have shown higher sensitivity for LN detection on a patient level [7–9, 28], none of these are sufficiently high to recommend preoperative PET/CT or PET/MRI examination to replace ePLND as a staging tool. This indicates that preoperative PET imaging plays a limited role as an alternative to ePLND in staging of high-risk prostate cancer patients.

In the ongoing discussion regarding the optimal treatment choice for LN-positive patients, there is growing evidence that treating stage N1 patients with surgery or

radiotherapy results in increased long-term survival [29–31]. In the current study, there were eight false-positive regions based on MRI, while none of these regions were suspicious based on PET uptake. The high specificity of ^{18}F-fluciclovine PET/MRI could be exploited to extend the resection area if the examination reveals a LN metastasis outside the surgical template. A highly specific N-staging tool is also important for selecting patients who are candidates for up-coming adjuvant therapies after radical prostatectomy.

We showed that there is a significant difference in size of metastatic LNs in PET false-negative and true-positive regions. The spatial resolution of the PET/MRI scanner used in this study is reported to be around 5 mm [32], and we noticed that the 75th percentile of false-negative lymph nodes is below this limit (Fig. 3). In theory, smaller metastasis could be detected if the tracer uptake is sufficiently high; however, this does not seem to be the case in this study. This is similar to PET/CT studies and studies using other tracers where micrometastases are not detected [18, 27].

The overall metastatic burden was higher in patients with positive PET findings compared to patients with negative scans in this study. Briganti et al. [33] demonstrated that patients with up to two positive nodes experienced significantly higher cancer-specific survival than patients with more than two positive nodes. In our cohort, none of the PET-negative patients had more than two metastatic LNs, and ^{18}F-fluciclovine PET/MRI could thus potentially help to stratify patients according to metastatic burden and support decisions regarding adjuvant therapy. In carefully selected patients (for instance patients with palpation findings indicating large tumour and/or stage T3b), a preoperative PET/MRI could add important information about the patient's metastatic burden without adding much time to a regular staging protocol.

Limitations

One inherent limitation of this study is the lack of per-LN analysis. It is practically impossible to identify every single LN described by histopathology in the images and therefore a region-based analysis was considered the best possible solution. In the case of several LN metastases per true-positive region, we assumed that the largest LN was visible in the images. Other limitations are the relatively low number of patients and the lack of a consensus reading between the radiologist and nuclear medicine physician for a combined PET/MRI score. Due to logistics it was not possible to fit this into the study design, and a retrospective assessment would not have been blinded to pathology results. We explored calculating a PET/MR score by simply combining the individual PET and MR scores ('PET and/or MR'), but the results did not differ from the individual PET and MR scores and the results were therefore not reported. We realize that we do not fully exploit the potential of the combined examination with this approach. Finally, two readers evaluated MRI while only one evaluated PET images, possibly giving a positive bias to the MRI. However, the radiologist in training had only limited experience in uro-radiology.

Conclusion

In conclusion, simultaneous ^{18}F-fluciclovine PET/MRI provides high specificity but low sensitivity for detection of LN metastases in high-risk prostate cancer patients. A ^{18}F-fluciclovine PET/MRI scan positive for LN metastases indicates a higher metastatic burden compared to a negative scan, and could warrant adjuvant therapy.

Compliance with ethical standards Guarantor

The scientific guarantor of this publication is Tone F. Bathen, NTNU – Norwegian University of Science and Technology, Faculty of Medicine and Health Sciences.

Conflict of interest The authors of this manuscript declare no relationships with any companies whose products or services may be related to the subject matter of the article.

Funding This study has received funding by 'The Norwegian Cancer Society' and 'The Liaison Committee between the Central Norway Regional Health Authority (RHA) and NTNU'.

Statistics and biometry No complex statistical methods were necessary for this paper.

Informed consent Written informed consent was obtained from all subjects (patients) in this study.

Ethical approval Institutional Review Board approval was obtained.

Study subjects or cohorts overlap Some study subjects or cohorts have been previously reported in Elschot, M., et al., *A PET/MRI study towards finding the optimal [18F]Fluciclovine PET protocol for detection and characterisation of primary prostate cancer.* Eur J Nucl Med Mol Imaging, 2017

Methodology
- prospective
- diagnostic or prognostic study
- performed at one institution

References

1. Hovels AM, Heesakkers RA, Adang EM et al (2008) The diagnostic accuracy of CT and MRI in the staging of pelvic lymph nodes in patients with prostate cancer: a meta-analysis. Clin Radiol 63:387–395

2. Heidenreich A, Bastian PJ, Bellmunt J et al (2014) EAU guidelines on prostate cancer. part 1: screening, diagnosis, and local treatment with curative intent-update 2013. Eur Urol 65:124–137
3. Briganti A, Chun FK, Salonia A et al (2006) Complications and other surgical outcomes associated with extended pelvic lymphadenectomy in men with localized prostate cancer. Eur Urol 50:1006–1013
4. Sankineni S, Brown AM, Fascelli M et al (2015) Lymph node staging in prostate cancer. Curr Urol Rep 16:30
5. Schuster DM, Nieh PT, Jani AB et al (2014) Anti-3-[(18)F]FACBC positron emission tomography-computerized tomography and (111)In-capromab pendetide single photon emission computerized tomography-computerized tomography for recurrent prostate carcinoma: results of a prospective clinical trial. J Urol 191:1446–1453
6. Turkbey B, Mena E, Shih J et al (2014) Localized prostate cancer detection with 18F FACBC PET/CT: comparison with MR imaging and histopathologic analysis. Radiology 270:849–856
7. Poulsen MH, Bouchelouche K, Hoilund-Carlsen PF et al (2012) [18F]fluoromethylcholine (FCH) positron emission tomography/computed tomography (PET/CT) for lymph node staging of prostate cancer: a prospective study of 210 patients. BJU Int 110:1666–1671
8. Beheshti M, Imamovic L, Broinger G et al (2010) 18F choline PET/CT in the preoperative staging of prostate cancer in patients with intermediate or high risk of extracapsular disease: a prospective study of 130 patients. Radiology 254:925–933
9. Maurer T, Gschwend JE, Rauscher I et al (2016) Diagnostic Efficacy of (68)Gallium-PSMA Positron Emission Tomography Compared to Conventional Imaging for Lymph Node Staging of 130 Consecutive Patients with Intermediate to High Risk Prostate Cancer. J Urol 195:1436–1443
10. Odewole OA, Tade FI, Nieh PT et al (2016) Recurrent prostate cancer detection with anti-3-[(18)F]FACBC PET/CT: comparison with CT. Eur J Nucl Med Mol Imaging 43:1773–1783
11. Nanni C, Zanoni L, Pultrone C et al (2016) (18)F-FACBC (anti1-amino-3-(18)F-fluorocyclobutane-1-carboxylic acid) versus (11)C-choline PET/CT in prostate cancer relapse: results of a prospective trial. Eur J Nucl Med Mol Imaging 43:1601–1610
12. Oka S, Okudaira H, Yoshida Y, Schuster DM, Goodman MM, Shirakami Y (2012) Transport mechanisms of trans-1-amino-3-fluoro[1-(14)C]cyclobutanecarboxylic acid in prostate cancer cells. Nucl Med Biol 39:109–119
13. Okudaira H, Nakanishi T, Oka S et al (2013) Kinetic analyses of trans-1-amino-3-[18F]fluorocyclobutanecarboxylic acid transport in Xenopus laevis oocytes expressing human ASCT2 and SNAT2. Nucl Med Biol 40:670–675
14. Sorensen J, Owenius R, Lax M, Johansson S (2013) Regional distribution and kinetics of [18F]fluciclovine (anti-[18F]FACBC), a tracer of amino acid transport, in subjects with primary prostate cancer. Eur J Nucl Med Mol Imaging 40:394–402
15. Elschot M, Selnaes KM, Sandsmark E et al (2017) A PET/MRI study towards finding the optimal [18F]Fluciclovine PET protocol for detection and characterisation of primary prostate cancer. Eur J Nucl Med Mol Imaging 44:695–703
16. (2016) FDA Approves 18F-Fluciclovine and 68Ga-DOTATATE Products. J Nucl Med 57:9N
17. Schuster DM, Votaw JR, Nieh PT et al (2007) Initial experience with the radiotracer anti-1-amino-3-18F-fluorocyclobutane-1-carboxylic acid with PET/CT in prostate carcinoma. J Nucl Med 48:56–63
18. Suzuki H, Inoue Y, Fujimoto H et al (2016) Diagnostic performance and safety of NMK36 (trans-1-amino-3-[18F]fluorocyclobutanecarboxylic acid)-PET/CT in primary prostate cancer: multicenter Phase IIb clinical trial. Jpn J Clin Oncol 46:152–162
19. Inoue Y, Asano Y, Satoh T et al (2014) Phase IIa Clinical Trial of Trans-1-Amino-3-(18)F-Fluoro-Cyclobutane Carboxylic Acid in Metastatic Prostate Cancer. Asia Ocean J Nucl Med Biol 2:87–94
20. D'Amico AV, Whittington R, Malkowicz SB et al (1998) Biochemical outcome after radical prostatectomy, external beam radiation therapy, or interstitial radiation therapy for clinically localized prostate cancer. JAMA 280:969–974
21. Joniau S, Van den Bergh L, Lerut E et al (2013) Mapping of pelvic lymph node metastases in prostate cancer. Eur Urol 63:450–458
22. Cardillo G (2006) Clinical test performance: the performance of a clinical test based on the Bayes theorem
23. Soret M, Bacharach SL, Buvat I (2007) Partial-volume effect in PET tumor imaging. J Nucl Med 48:932–945
24. Axumin (fluciclovine F 18) Injection, Printed Labeling Available via https://www.accessdata.fda.gov/drugsatfda_docs/nda/2016/208054Orig1s000Lbl.pdf
25. Lyons K, Seghers V, Sorensen JI et al (2015) Comparison of Standardized Uptake Values in Normal Structures Between PET/CT and PET/MRI in a Tertiary Pediatric Hospital: A Prospective Study. AJR Am J Roentgenol 205:1094–1101
26. Schiavina R, Scattoni V, Castellucci P et al (2008) 11C-choline positron emission tomography/computerized tomography for preoperative lymph-node staging in intermediate-risk and high-risk prostate cancer: comparison with clinical staging nomograms. Eur Urol 54:392–401
27. Steuber T, Schlomm T, Heinzer H et al (2010) [F(18)]-fluoroethylcholine combined in-line PET-CT scan for detection of lymph-node metastasis in high risk prostate cancer patients prior to radical prostatectomy: Preliminary results from a prospective histology-based study. Eur J Cancer 46:449–455
28. van Leeuwen PJ, Emmett L, Ho B et al (2017) Prospective evaluation of 68Gallium-prostate-specific membrane antigen positron emission tomography/computed tomography for preoperative lymph node staging in prostate cancer. BJU Int 119:209–215
29. Reyes DK, Pienta KJ (2015) The biology and treatment of oligometastatic cancer. Oncotarget 6:8491–8524
30. Engel J, Bastian PJ, Baur H et al (2010) Survival benefit of radical prostatectomy in lymph node-positive patients with prostate cancer. Eur Urol 57:754–761
31. Gakis G, Boorjian SA, Briganti A et al (2014) The role of radical prostatectomy and lymph node dissection in lymph node-positive prostate cancer: a systematic review of the literature. Eur Urol 66:191–199
32. Delso G, Furst S, Jakoby B et al (2011) Performance measurements of the Siemens mMR integrated whole-body PET/MR scanner. J Nucl Med 52:1914–1922
33. Briganti A, Karnes JR, Da Pozzo LF et al (2009) Two positive nodes represent a significant cut-off value for cancer specific survival in patients with node positive prostate cancer. A new proposal based on a two-institution experience on 703 consecutive N+ patients treated with radical prostatectomy, extended pelvic lymph node dissection and adjuvant therapy. Eur Urol 55:261–270